Topics in Catalysis
https://doi.org/10.1007/s11244-020-01365-1

ORIGINAL PAPER

Surface Reconstruction of Ag and Au–Ag Model Nano-catalysts During Exposure to Oxidising Gas Atmospheres

Luc Jacobs[1] · **Cédric Barroo**[1,2] · **Thierry Visart de Bocarmé**[1,2]

Abstract
At the industrial level, Ag catalysts in the form of silver crystals held by a silver gauze are largely used for formaldehyde production and ethylene epoxidation. These self-supported structures undergo surface reconstructions and morphological changes upon exposure to moderately high temperatures (473–900 K) and oxidising atmospheres. These phenomena have been studied and well understood on single crystal surfaces and polycrystalline foils: different oxygen surface and sub-surface species have been identified and reconstruction processes explained. To verify the scalability of the surface science results and ultimately understand these phenomena on catalysts at the industrial scale, further studies on more complex samples are needed. Attempts to close this "materials gap" have been carried out in this present study where experiments have been performed on model single catalytic nanoparticles, i.e. the apexes of field emitter tips, using both field emission (FE) and field ion (FI) microscopies. Pure Ag samples are exposed to a pressure of 3×10^{-5} mbar of O_2 at temperatures up to 700 K. These conditions reflect those used on the industrial scale. Important surface/morphological reconstructions are observed both in FE and FI modes. For comparison, experiments have been repeated on Au-8.8%at. Ag field emitter tips, representative samples for Au–Ag catalytic nanofoams, using to 3×10^{-5} mbar of NO_2 at temperatures up to 450 K. Similar behaviour are observed and the influence of the oxidising gas is discussed.

Keywords Field emission microscopy · Field ion microscopy · Nanocatalysis · Surface reconstruction · Gold-based catalysis · Silver

1 Introduction

Research in the domain of catalysis aims at understanding the complex interplays between the catalytic support, the multi-metallic active phase and the reactive gases to understand how catalysts change their composition, deactivate or even undergo structural and morphological changes upon reaction. But when one of the most successful industrially used catalyst for partial oxidation reactions is made of a single metal, i.e. self-supported catalyst, the support, and segregation related aspects become void and questions about the structural evolution during reaction turn out to be crucial. This is the case for pure Ag catalysts used in the industrial production of ethylene oxide and of formaldehyde from methanol. During these reactions, Ag crystals held on Ag grids are exposed to temperatures comprised between 473 and 523 K for ethylene epoxidation and between 543 and 900 K for formaldehyde production in presence of oxidising gases like oxygen [1–3]. Over the years, many research groups have exploited the surface science approach to get a fundamental understanding of the ongoing processes, extrapolate the results, and hence improve the performances at the industrial scale.

In such a way, relevant single crystal facets of Ag, e.g. (111), (100) and (110), have been thoroughly studied using different techniques (such as Auger Electron Spectroscopy (AES), Low Energy Electron Diffraction (LEED), Temperature Programmed Desorption Spectroscopy (TDS) or Scanning Tunnelling Microscopy (STM)). It was found that the reactive sticking coefficients for O_2 are actually very low, especially on Ag(111) (10^{-7} at 300 K [4, 5]), whereas they

✉ Luc Jacobs
lucjacob@ulb.ac.be

[1] Chemistry of Surfaces, Interfaces and Nanomaterials (ChemSIN) – Catalysis, Université Libre de Bruxelles, CP243 Brussels, Belgium

[2] Center for Nonlinear Phenomena and Complex Systems (CENOLI), Université Libre de Bruxelles, CP231 Brussels, Belgium

Published online: 04 September 2020

are significantly higher on Ag(100) (10^{-2}–10^{-3} [6–8]) and on Ag(110) (3×10^{-3} [5, 9, 10]) at the same temperature. At lower temperatures (100 K) and high incident kinetic energies of the incident molecules, these coefficients can be as high as 0.5 for Ag(100) and Ag(110) whereas the Ag(111) facet remains relatively inert [6–9]. Based on the interpretations of the sticking coefficients, one can therefore suggest that Ag(110) is the most suited facet for O_2 dissociation whereas Ag(111) can be considered as almost inert. The same conclusion has been found in first principles simulations and kinetic Monte-Carlo modelling [11].

Further efforts were made to identify the exact nature of the species present at the surface. In fact, temperature programmed desorption spectroscopy (TDS) experiments have shown that even in the case where Ag is simply exposed to 0.01–300 mbar O_2, rather complex phenomena occur, and a series of different species can form. Oxygen exposure of Ag leads to chemisorption of O(ads) in a large temperature window, from room temperature up to 900 K. This chemisorbed oxygen, also called O_α, can penetrate into the bulk of single crystal surfaces and is then called O_β [4, 5, 12, 13]. Furthermore, at high temperatures (800–900 K), O_β can re-diffuse towards the surface without immediate desorption. At these temperatures, the existence of a well-structured binary compound like Ag_2O oxide is excluded [14] since the temperature is higher than the thermodynamic decomposition temperature of Ag_2O [15]. This "surface-embedded" oxygen is referred to as O_γ. It has been shown that these O_γ species are of utmost importance in the catalytic mechanisms of Ag catalysed oxidation reactions in these temperature ranges [4, 14, 16, 17]. Moreover, O_γ is stable at the surface even at temperatures over 900 K and a maximum rate of O_γ formation is observed at 820 K.

From a structural point of view, LEED experiments in reduced pressure conditions ($\approx 10^{-5}$ mbar O_2) and temperatures ranging from room temperature to 600 K have shown that O_2 exposure can lead to different structures. Adsorption and formation of superstructures is found on the (100) and (110) facet whereas the clean and well ordered (111) facets remains practically inert. Under these conditions, no bulk diffusion of oxygen has been observed [9]. Moreover, it could be shown that the presence of surface defects significantly changed the properties of the (111) facet, highlighting the importance of structural defects. Low coordinated surface atoms then act as an "entry gate" for oxygen atoms [9]. This also shows that, as compared to the TPD experiments presented above, the onset of oxygen bulk diffusion and the formation of subsurface oxygen lies above 600 K on single crystals under reduced pressure conditions, $\approx 10^{-5}$ mbar O_2, as compared to the higher pressures used in TDS (0.01 – 300 mbar). Rovida et al. have shown that in similar temperature ranges but higher pressures (10^{-3}—1 mbar and 293—773 K), the Ag(100) and Ag(110) surface reconstruct and expand via a faceting process after exposure to 10^{-1} mbar of O_2 at 423 K during 10 min, whereas on the Ag(111) facet, the formation of a thermally reversible (4×4) O_2 superstructures is observed [18, 19].

Upon oxygen exposure at temperatures above 600 K, single crystal surfaces of Ag can therefore be decorated with different oxygen species, chemisorbed O_α, subsurface O_β and surface embedded, highly reactive O_γ. Moreover, structural changes can occur, especially on the (100) and (110) facets, whereas the dense (111) facet shows again the least sensibility.

The insights from single surface studies have been translated on more complex samples like polycrystalline Ag foils. Nagy et al. and Bao et al. showed that the heating of Ag foils under ultra high vacuum (UHV) leads to the formation of (012) faceting, whereas the exposure of Ag foils to O_2 gas and O_2 + methanol gas mixtures at 920 K induces surface reconstructions towards flat terraces and parallel facets [12, 20]. Similar observations have been made by Herein et al. who reported the reconstruction of (110)-oriented domains in polycrystalline foils after the exposure to 0.01 – 300 mbar of O_2 at 525–1000 K accompanied by the formation of channels perpendicular to the (110) surface, allowing for oxygen diffusion [14]. Complementary thermal desorption spectroscopy experiments have proven the presence of three different oxygen species with distinctive desorption properties, as reported on single crystal surfaces. The presence of gas phase oxygen, and the availability of low resistance diffusion paths towards the Ag bulk guarantee a constant formation of sub-surface O_β, and hence the presence of O_γ, at the reaction temperatures situated around and above the actual desorption temperatures of O_β and O_γ, an important point to explain the catalytic activity of these catalysts at high temperature [10, 12, 14].

Nonetheless, there is a discrepancy in the used pressures between the single crystal surface experiments, the experiments on Ag foils and high-pressure experiments, as well as applied conditions in the industry. The issue of this "qualitative pressure gap between 10^{-4} and 10 mbar" has already been discussed in the past [14]. For numerous surface science techniques, it is not possible to work at higher pressures than 10^{-4}–10^{-3} mbar range for technical reasons. However, narrowing the materials gaps, i.e. using samples with higher structural complexity, without losing the high resolution of surface science techniques can allow to verify the prerequisites made on single crystals and foils on samples which are a step closer to the complexity of industrially used catalysts.

This approach has been exploited by different research groups with the same experimental techniques used in this paper, i.e. field emission techniques which comprises field emission microscopy and field ion microscopy. Single model catalytic nanoparticles prepared as sharp tips are imaged at cryogenic temperatures in field

ionisation (FI) mode to reveal the surface structure with atomic resolution and at reaction temperatures in presence of reactive gases in field emission (FE) mode to study the reactivity of the used materials. Schmidt et al. have reported field emission micrographs of clean and contaminated Ag field emitter samples without addressing surface reconstructions or morphological changes upon the exposure of reactive gases [21]. Czanderna et al. have exposed Ag field emitter tips to oxygen at different temperatures (100–473 K) and exposure times, and changes in the emission properties have been observed in FE mode only. These changes are not imaged in FI mode and the applied temperatures are significantly lower than the conditions applied industrially [22]. Janssen et al. have reported darkening of the field emission pattern during the exposure of Ag samples to O_2 up to 473 K. This is linked to an increase of the surface work function following O_2 dissociative adsorption over the structurally open (012) facets. The general darkening extends then over the (110) zone lines and, ultimately, the (111) facets becomes smaller with the formation of bright rings around them. Besides these reports on work function changes upon face-specific oxygen adsorption and dissociation, no reports on the possible surface reconstructions or corresponding FI images have been presented [23].

In this paper, we exposed Ag field emitter samples to O_2 atmospheres in the 300–700 K temperature range, range selected to obtain results representative of the industrially applied temperatures used for ethylene epoxidation and formaldehyde production. To set against the reduced pressure conditions far from applied conditions, field emitter samples are used as representative models for the real used catalysts, as well for the size as for the multitude of different crystallographic facets exposed on a single sample. The complexity of the sample is therefore similar to the real catalysts. As a comparison and extension of the study, a second catalytic system, Au-8.8%at. Ag is studied in presence of NO_2 as oxidising gas. Applied formulations of these catalysts are also made of metallic unsupported nanoporous structures [24–26]. The highly crystalline ligaments found in such systems can be represented by field emitter tips of similar sizes. For these catalysts, the presence of oxygen atoms at the surface is also a crucial factor to explain the reactivity, and their influence on the structural evolution during reaction is equally important. The goal of these experiments is to image the surface reconstructions and morphological changes observed on comparatively large single crystals and foils, in similar temperature conditions and reduced pressure environments, but on single catalytic nanoparticles which are more representative of the industrially used catalysts.

2 Experimental

The experiments are carried out in an ultrahigh vacuum setup capable of imaging samples both in Field Ion Microscopy (FIM) and Field Emission Microscopy (FEM) modes. A specifically adapted gas inlet system allows to introduce gases required for imaging and for physicochemical treatments using different high precision leak valves. Au (99.99 at.%) and Au-8.8%at. Ag samples are prepared in the form of very sharp tips with a final diameter of 20–50 nm. This size range is close to the upper limit of our microscope as from a technical point of view one can only apply a limited voltage (10 kV), but this size range also guarantees the good correlation between the used samples and real catalytic nanoparticles. The preparation of the sample is achieved by micro-electropolishing a 0.1 mm wire of the mentioned materials in an aqueous solution of KCN (20 wt.%) under the application of a continuous voltage of 4–7 V. The structural integrity of the as formed tips is verified by optical microscopy, followed by in-situ development steps in the microscope. Amongst these steps are field evaporation of the outermost atomic layers with the intention of shaping the sample to its final hemispherical form and flash heating aiming at the desorption of impurities and adsorbates. After these in-situ development steps, it is eventually possible to obtain micrographs illustrating the crystallographic symmetries of the used samples, or even individual crystallographic facets and surface atoms in favourable conditions.

In FE mode the characterisation is possible thanks to the local work functions of different crystallographic facets. Like this, upon increasing the electric field near the surface (negative polarity on the sample) between the sample and the imaging screen, low work function – "open" type crystallographic facets emit electrons and are the first to appear bright, whereas high work function – "dense" crystallographic facets remain dark. This relationship between the surface work function (ϕ), the electric field (F) and the emission current (I) is known as Fowler–Nordheim equation [27, 28] (1):

$$I = A \cdot a \frac{F^2}{\phi} \exp\left(\frac{-b \cdot \phi^{3/2}}{F}\right) \tag{1}$$

where A is defined as the emission surface (considered crystallographic facet) and a, b are constants. The obtained FE micrographs therefore represent a two-dimensional map of the electron emission probabilities of the used sample with respect to the work functions of the exposed facets.

In FI mode, an imaging gas can be used to reveal the surface structure with atomic resolution. In fact, the application of a high electric field (positive polarity on the sample) triggers the ionisation of the imaging gas atoms over the surface of the sample, and more precisely, exactly over

surface atoms where the local electric field is the highest due to the increased local curvature of the surface atom itself. The formed positively charged ions are repelled towards the phosphorescent imaging screen facing the sample, following, as a first approximation, the electric field lines, and giving rise to a FI pattern with atomic resolution under favourable conditions.

When combining the information of the symmetric FE pattern with the atomic resolution FI micrographs and comparing both to theoretically calculated stereographic projections, it is possible to assign the Miller indices of the facets exposed by the sample. This is important for the evaluation of structural differences occurring at the surface of the catalyst before, during and after reaction. Therefore, in our case, both techniques are well-suited to follow the surface structure and morphology of model catalytic nanoparticles.

3 Results and Discussion

3.1 Ag Exposure to O_2

The Ag model nanoparticle used in the first set of experiments has an estimated diameter of 36 nm. This evaluation is made using Eq. (2) expressing the relationship between the electric field (F), the applied voltage (V), the radius of the sample (r) and a geometrical constant (k) proper to each microscope (12 in our case).

$$r = \frac{V}{k \cdot F} \tag{2}$$

To obtain a correct diameter, one should be careful that at the moment of the size estimation, only field ionisation of H_2, i.e. imaging of the sample, occurs and no field evaporation of Ag. In such a way, the electric field present is considered equal to the ionisation field of H_2, used as imaging gas rather than the evaporation field of Ag. Together with the applied voltage and the geometrical constant k, a correct estimation of r is obtained.

Prior to any physicochemical treatments, the sample was developed in-situ using field evaporation (i.e. at a higher electric field than used for imaging only), flash heating and then imaged both in FI and FE mode at cryogenic temperatures. The obtained pictures are shown in Fig. 1a, b, respectively. It should be mentioned that the quality of the FI micrograph shown in Fig. 1a is certainly poorer than almost perfectly developed textbook examples of Rh or W samples found in the literature. The main reason for this is the use of H_2 as imaging gas, with a rather weak localization of field-adsorbed H_2 as compared to commonly used Ne or He. On the one hand this illustrates the challenging nature of preparing Ag samples for field emission microscopy and surely complicates the attribution of Miller indices to the observed facets. As compared to Au, Ag oxidises easier and is therefore more susceptible to be covered with impurities, moreover the evaporation field of ≈ 22 V/nm is close the imaging field of H_2. On the other hand, a slightly less developed model nanoparticle is certainly closer to a "real" supported catalytic Ag nanoparticle, and therefore an even more realistic model nanoparticle with the presence of many surface defects. Nonetheless, there is strong correlation between the pattern observed in Fig. 1a, b. The bright facets in Fig. 1b most probably correspond to {011} facets based on comparisons with a (111) orientated stereographic projection of the fcc crystal structure. On micrographs published in previous studies by our group analysing the NO adsorption on Ag field emitter tips, the {011} facets had also been attributed the most important brightness during imaging in FI mode [29]. The sample was then left to "heat" up to room temperature upon which the FE pattern changed. No physicochemical treatments other than the gradual warming of the sample (over 24 h) were made between the snapshots presented Fig. 1b–d. However, significant changes in the FE pattern can be observed. To explain this, it should first be said that the FE pattern in Fig. 1b corresponds to the FE pattern of a freshly field evaporated, rough, and structurally "frozen" surface. During the warming up to room temperature (Fig. 1c, d), the mobility of the surface species is significantly increased which results in a "surface-relaxation" a diminishment of the surface free energy as compared to the frozen state in Fig. 1a which corresponds to the quasi-hemispherical field-evaporated end form. Consequently, the {011} facets split into their geographical neighbouring {012} facets. Typical FE pattern of clean, fcc-(111) orientated field emitter tips show emission of electrons through six {012} facets, (linked to the symmetry properties of a (111) orientated fcc crystal). The {012} facets exhibit the lowest work function for Ag, therefore emit electrons first upon increasing of the electric field and can hence be identified, like in picture Fig. 1c. The difference between Fig. 1.c and Fig. 1.d is an additional 24 h of resting under UHV conditions, at room temperature, and an increased imaging voltage of about 7%. Next the surface has been exposed to 3×10^{-5} mbar of O_2 at 700 K during 40 min, the surface reconstruction is considerable and can be observed in both FI and FE modes.

The first surface modification corresponds to a surface relaxation triggered by the temperature raising from cryogenic to room temperature (Fig. 1b–d). Even with a poorly developed FI image (as presented in Fig. 1a), this change allows to attribute Miller indices to the visible facets. A second change is observed following the oxidising treatment (3×10^{-5} mbar of O_2, 700 K, 40 min) where drastic changes in the FI and FE micrographs can be noted. Overall, a general darkening of the FE pattern is remarked. This evolution is in line with the expected work

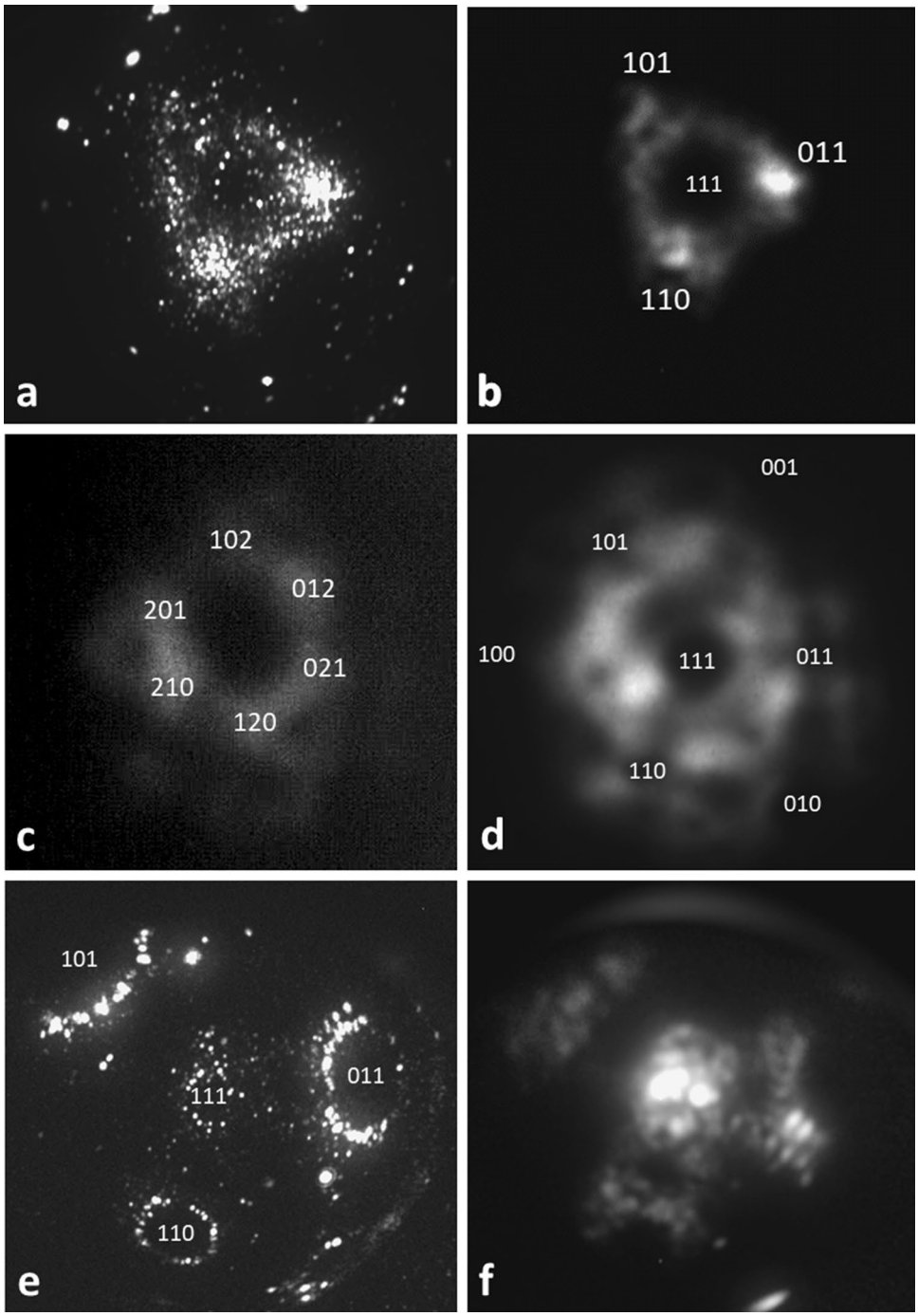

Fig. 1 **a** Field ion micrograph of a clean Ag sample imaged using hydrogen with an estimated radius of curvature of 36 nm. Conditions of acquisition: T = 63 K, P = 8×10^{-6} mbar, F = 22 V/nm; **b** Field emission pattern of the same sample imaged under UHV conditions showing the emission of electron through the facets with a rough, open surface structure, presumably {011} facets. Conditions of acquisition: T = 62 K, P < 1×10^{-8} mbar, F ≈ 4 V/nm; **c** FE pattern following the "surface-relaxation" of the sample with bright areas correspond to low work function zones of electron emitting (012) facets. Conditions of acquisition: T = 300 K, P < 1×10^{-8} mbar, F ≈ 4 V/nm; **d** FE micrograph after an additional 24 h of resting at room temperature: an increased electric field leads to a larger visible area of the sample. Conditions of acquisition: T = 300 K, P < 1×10^{-8} mbar, F ≈ 4.3 V/nm; **e** FI micrograph and **f** FE of the same Ag sample following the exposure to 3×10^{-5} mbar of O_2 at 700 K during 40 min. The symmetry properties are conserved but a surface reconstruction over the {011} facets in the form of a facet extension can clearly be noticed. Moreover, the bright {012} crown and central (111) facet have inverted their brightness properties following the treatment and the necessary electric field for imaging has significantly increased. Conditions of acquisition: **e** T = 63 K, P = 1×10^{-7} mbar, F = 22 V/nm; **f** T = 62 K, P < 1×10^{-8} mbar, F ≈ 8–9 V/nm

function changes upon oxygen adsorption on Ag [23] and is reflected in an increased applied potential to recover similar brightness levels.

A comparison of the FI micrographs Fig. 1a, e as well as the FE micrographs Fig. 1d, f shows that all three (011) facets are subject to an expansion and bright circular forms. Moreover, the central (111) facet, initially dark, becomes bright and the initially bright crown composed of high index planes (mostly {012} and {133}) is now darkened. Several prerequisites must be established to understand these three qualitative changes.

First of all, the darkening of the initially bright {012} crown. The behaviour of oxygen adsorption at 473 K on structurally open facets, like {012} and {133} with a general increase of the surface work function has already been reported on field emitter tips and single crystals [8, 9, 21, 22, 29]. On the open reactive {012} and {133} facets, dissociative adsorption of oxygen covers the surface with

chemisorbed oxygen atoms and subsequently darkens these facets. It has been shown that at temperatures sufficiently high, typically at the experimental conditions used here, chemisorbed oxygen, sometimes also referred to as O_α, can penetrate the bulk [4, 5, 12, 13] following defects or structurally open facets, like (012). This process has been explained in the introduction part. After bulk diffusion these oxygen atoms are defined as O_β. This concept is important for the explication of the following observations.

Second, the three visible {011} facets have clearly increased in size. To understand this morphological reconstruction, various values of molecular and reactive sticking coefficients of Ag(111), Ag(100) and Ag(110) facets, as well as the corresponding energy barriers for dissociation, are summarised in Table 1.

It can clearly be seen that the (110) facet is the most reactive for O_2 dissociation [8, 11]. This means that under the used experimental conditions, O(ads) has a tendency to bind to surface atoms of the (110) facets. Moreover, the (110) facet has the lowest work function amongst these three facets (Ag(111): $\phi = 4.74$ eV > Ag(100): $\phi = 4.64$ eV > Ag(110): $\phi = 4.52$ eV) and the adsorption of oxygen therefore stabilises these facets and explains their increasing size during the experiment. Also, the temperature range of the experiments lies above Tamman temperature, defined as the temperature above which bulk diffusion of a metal is such that significant mass transport within the timescales of the performed experiments is observed. In this case, this is equivalent to the formation of new facets during the oxidising treatment. For silver, the Tamman temperature is given between 620 – 770 K for Ag [8, 32, 33]. This means that we work at temperatures where mass transport (Ag surface diffusion) is possible and kinetically fast enough to observe the size increase of the Ag(110) facets.

Third, after the oxidising treatment, the initially dark Ag(111) facet is completely bright. To understand how a dark, dense, high work function facet with an extremely low reactive sticking coefficient for O_2 (see Table 1) becomes bright, we need to go back to the first point and use the results of preliminary published studies on single crystal Ag surfaces. It is an established fact that defects or structurally open facets can act as entry gates for bulk diffusion of oxygen [9, 10, 12, 14, 20]. It has been reported that heating of a O(ads) pre-covered surface can lead to bulk diffusion of oxygen at temperatures as low as 473 K (reported between 412 and 862 K [4, 5, 12, 13]. Not only is this temperature condition fulfilled, but the {012} facets also guarantee the presence of O(ads) at the surface of our sample. It is hence possible for oxygen atoms to diffuse laterally under the Ag(111) facet as subsurface oxygen. When O(ads) is located on the surface, the induced dipole increases the work function of the surface, when present as subsurface oxygen under the 1st till 4th atomic layers the dipole is inverted, and the work function decreases. At the same time, the low sticking coefficient and high temperatures guarantee the absence of O(ads) on the surface of Ag(111). This behaviour of subsurface oxygen has already been reported on single crystal surfaces and single catalytic nanoparticles [13, 34].

3.2 Au-8.8%at. Ag Exposure to NO_2

A similar experimental approach has been used to study Au-8.8%at. Ag samples. As explained, these samples are representative models for Au–Ag nanoporous catalysts and have been chosen to highlight the role of silver atoms embedded in a relatively inactive gold matrix. Nonetheless, it has been shown that the catalytic contribution of silver is crucial [35, 36]. As compared to pure Au [37–39], Ag has much stronger interactions with oxygen [40, 41] and can therefore be considered as the atomic oxygen provider in Au–Ag based catalysis for oxidation reactions.

In our case, the presence of Ag in the field emitter tips has proven to be sufficient to lead to a general darkening of the FE pattern, due to dissociative adsorption of O_2, a process that does not occur on pure Au field emitter tips. However, these treatments do not induce surface reconstructions observable within the achievable nanoscale resolution of FEM and are therefore not represented. To countermeasure for this situation, one could increase the Ag content in the sample (to increase the probability of O_2 dissociation) or increase the oxidising power of the reactive gases (leading to the formation of O(ads) even on a chemically inert—Au rich surface). To keep the representativity of the Au-8.8%at. Ag sample with respect to largely used Au–Ag nanofoams (and their minor Ag content), it was chosen to use NO_2 as an oxidising gas rather than field emitter samples with increased

Table 1 Summary of various coefficients relevant to the comprehension of the physicochemical phenomena in play during O_2 / Ag field emitter tips interactions

Molecular sticking coefficient: O_2 (ads)	Reactive (dissociative) sticking coefficient: $O_2 \rightarrow 2$ O(ads)	Energy barrier for O_2 dissociation:
Ag(111) = 10^{-6} at 150 K [9] Ag(111) = 10^{-7} at 300 K [30]	Ag(111) = 10^{-6} at 150 K [30, 31] Ag(111) = 10^{-7} at 298 K [5, 12]	Ag(111) = 1.1 eV [8]
Ag(100) = 0.5 at 100 K [7] Ag(100) = 10^{-2} – 10^{-3} at 300 K [6, 7]	Ag(100) = 10^{-4} at 298 K [5, 12]	Ag(100) = 1.1 eV [8]
Ag(110) = 0.5 at 100 K [6] Ag(110) = 3×10^{-3} at 300 K [9]	Ag(110) = 10^{-3} at 298 K [5, 12]	Ag(110) = 0.36 eV [8]

Ag content. Moreover, NO_2 is used in surface science as an O(ads) species provider or during pre-treatments of catalysts such as Au–Ag nanofoams for the selective segregation of Ag towards the surface [42].

Images of a freshly field evaporated Au-8.8%at. Ag field emitter tip can be seen in Figs. 2a and 3a. Four bright regions can be discerned corresponding to a four-fold symmetry of a (001) orientated fcc crystal. Already published

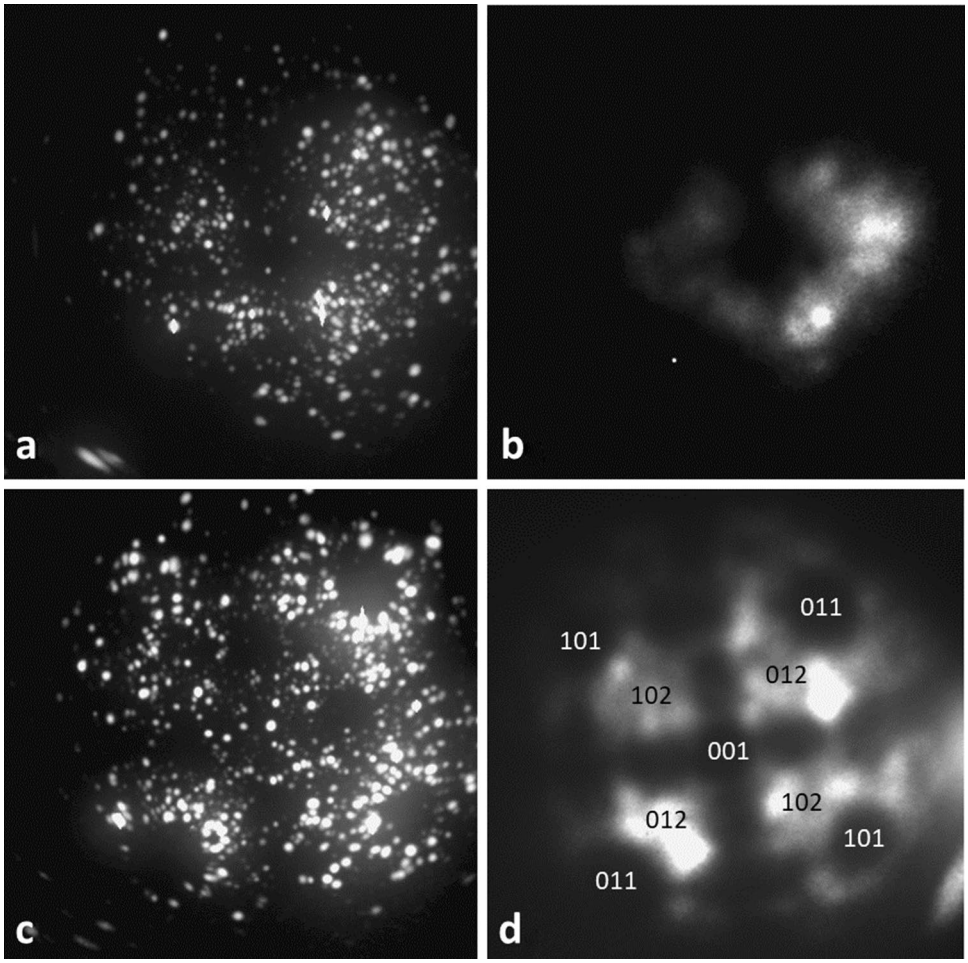

Fig. 2 **a** Field ion micrograph of a clean Au-8.8%at. Ag sample imaged using hydrogen with an estimated radius of 24 nm. Conditions of acquisition: T = 65 K, $P = 1 \times 10^{-5}$ mbar, F = 22 V/nm; **b** Field emission pattern of the same sample imaged in UHV showing the emission of electron through the facets exposing the lowest work function. Conditions of acquisition: T = 65 K, $P < 1 \times 10^{-8}$ mbar, F ≈ 4–5 V/nm; **c** FI micrograph and **d** FE micrograph of the same Au-8.8%at. Ag sample following the exposure to 3×10^{-5} mbar of NO_2 at 500 K during 1 h. The symmetry properties are conserved but a surface reconstruction of the bright open facets in the form of a facet extension can clearly be noted. Conditions of acquisition: **a** T = 63 K, $P = 1 \times 10^{-7}$ mbar, F = 22 V/nm; **d** T = 300 K, $P < 1 \times 10^{-8}$ mbar, F ≈ 6 V/nm

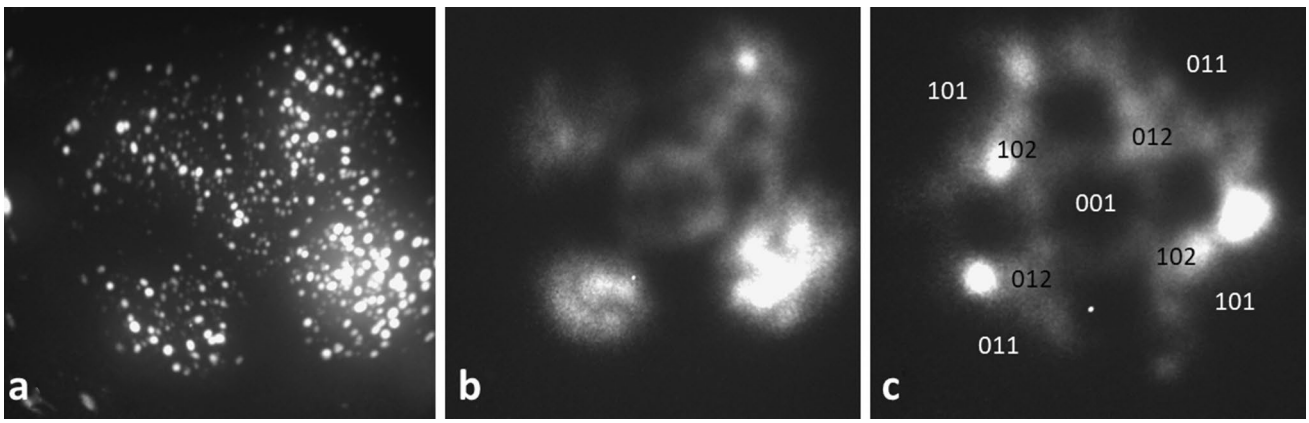

Fig. 3 Series of micrographs showing a second exposure of a freshly field evaporated Au-8.8%at. Ag sample to illustrate the reproducibility of the surface reconstructions induced at 500 K in presence of 3×10^{-5} mbar of NO_2. Conditions of acquisition: **a** T = 65 K, $P = 1.5 \times 10^{-6}$ mbar, F = 22 V/nm; **b** T = 300 K, $P < 1 \times 10^{-8}$ mbar, F ≈ 5 V/nm, **c** T = 300 K, $P < 1 \times 10^{-8}$ mbar, F ≈ 6 V/nm

FI micrographs prove that alloy Au–Ag single crystal can be obtained and imaged with atomic resolution [43]. The radius of the tip is estimated to 24 nm, based on the same procedure as already explained. The corresponding FE pattern shown in Figs. 2b and 3b present a very good correlation. The Au-8.8%at. Ag sample has then been exposed to 3×10^{-5} mbar of NO_2 at 500 K during 1 h, leading to changes in the FI and FE pattern as shown in Figs. 2c, d and 3c. Besides the qualitative change in the pattern of the micrographs, an increased imaging voltage is also necessary following the increased work function after NO_2 dissociative adsorption.

Figure 3 shows a second experimental dataset obtained under identical experimental conditions. Prior to performing this experiment, the sample was field evaporated in FI mode at cryogenic temperatures to ensure identical starting conditions for the experiment, as well from a structural as from a compositional point of view.

As observed for pure Ag, an extension of the {011}facets can clearly be noted, nonetheless to a lesser extent. This is accompanied by a qualitative inversion of their brightness, from initially bright to dark. This can be explained by the relative high interactions of O(ads) with the {011} oriented facets, as well as a lateral diffusion of O(ads) towards these facets. An observation which is fundamentally different from the results obtained on bare Ag samples are the {012} facets which remain bright. These structurally open facets are prone to dissociative adsorption of gases, especially O_2 and NO_2, at this stage it is challenging to advance a hypothesis on why the presence of O(ads) seems not to influence the emission properties of these facets.

In oxidising conditions, the presence of O(ads) at the surface of Au–Ag alloys can induce surface segregation of Ag, due to differing interactions, as explained above. This is presumably the case here as such behaviour has already been demonstrated by atom probe tomography (APT) experiments where Au-8.8%at.Ag sample were exposed to N_2O at 423 K [44], N_2O being used there as an atomic oxygen provider. Therefore, similar or enhanced surface segregation behaviours are expected using O_2 and NO_2 as oxidizing gas. The experiments presented here confirm the presence of changes at the surface of Au–Ag catalysts in oxidising conditions observed in APT, but this time visually as FE techniques are a purely imaging microscopy. Nonetheless this shows the importance to fundamentally understand the nanoscale changes that occur at the surface of catalysts during activation or pre-treatment from a compositional and structural point of view. In our case, the NO_2 treatment could even induce regio-selective surface segregation of Ag towards the {011} facets. The relative increased Ag surface concentration could lead to improved interactions with O(ads) and explain the absence of electron emission through these facets under the given conditions. These hypotheses would need further investigations using atom probe tomography with a large field of view. At this stage, they cannot be proven.

4 Conclusion

The presented experiments carried out on pure Ag and Au-8.8%at. Ag aimed at the imaging of surface reconstructions occurring under oxidising gas exposure at reduced pressure on samples and in temperature conditions relevant to those found in the industry, especially in the context of formaldehyde production and ethylene epoxidation, so as to narrow the "materials gap". We worked in conditions and with gases where face-selective and random dissociative adsorption is possible; where lateral diffusion of adsorbates and surface atoms is possible; and where bulk diffusion of adsorbates occurs. Using established prerequisites obtained in surface science on single crystal surfaces, we could fully explain the observations made on pure Ag and to some extent those on Au-8.8%at. Ag. On Ag, dissociative adsorption of O_2 leads to chemisorbed O_α, decreasing the overall work function, and available to bulk-diffuse through open type facets leading to inverted surface dipole situations as observed for the Ag(111) facet. At the conditions used this O_β can diffuse back to the surface where it is strongly bound as O_γ and together with favourable interactions between O(ads) and the {011} facets induce a stabilisation and a net size increase of the {011} facets. On Au-8.8%at. Ag the limited quantity of Ag is not sufficient to provide equal amounts of O(ads) at the surface of the sample, and the gas atmosphere must contain strongly oxidizing species such as NO_2 to observe similar phenomena. This is possible due to the surface diffusion of O(ads).

The results presented here show that field emitter tips are relevant samples to image surfaces and surface reconstructions with nanoscale or even atomic scale resolution, and that the combination of these results with information obtained using UHV-based surface science experiments allow to get a better understanding of the behaviour of such catalyst under industrially relevant conditions. Ultimately this information can be important in the context of shape specific synthesis of increasingly active catalytic nanoparticles.

Author contributions Funding of the project: L.J., C.B., T.V., Design and realisation of the experiments: L.J., C.B., Interpretation of the data: L.J., C.B., Manuscript writing: L.J., Manuscript review, L.J., C.B., T.V.

Funding Luc Jacobs and Cédric Barroo thank the Fonds de la Recherche Scientifique (F.R.S.-FNRS) for financial support: PhD grant from FRIA (L.J.) and postdoctoral fellowship from FNRS (C.B.).The authors thanks Dr. Eric Genty for fruitful discussions.

Compliance with Ethical Standards

Conflict of interest All authors declare that they have no conflict of interest.

Data Availability of Data and Material All used materials are commercially available. Precise information on the presented data are available upon request.

References

1. Andreasen A, Lynggaard H, Stegelmann C, Stoltze P (2005) Appl Catal A 289:267–273
2. van Santen RA, Kuipers HPCE (1987) Adv Catal 35:265–321
3. Bahmanpour AM, Hoadley A, Tanksale A (2014) Rev Chem Eng 30(6):583–604
4. Bao X, Muhler M, Schedel-Niedrig Th, Schlögl R (1996) Phys Rev B 54(3):2249–2262
5. Li W-X, Stampfl C, Scheffler M (2002) Phys Rev B 65:075407
6. Vattuone L, Rocca M, Boragno C, Valbusa U (1994) J Chem Phys 101:713–725
7. Buatier de Mongeot F, Rocca M, Valbusa U (1996) Surf Sci 363:68–72
8. Loncaric I, Alducin M, Juaristi JI (2015) Phys Chem Chem Phys 17:9436
9. Engelhardt HA, Menzel D (1976) Surf Sci 57:591–618
10. Outlaw RA, Wu D, Davidson MR, Hoflund GB (1992) J Vac Sci Technol, A 10:1497
11. Hus M, Hellman A (2019) ACS Catalysis 9:1183–1196
12. Nagy AJ, Mestl G, Herein D, Weinberg G, Kitzelmann E, Schlögl R (1999) J Catal 182:417–429
13. Xu Y, Greeley J, Mavrikakis M (2005) J Am Chem Soc 127:12823–12827
14. Herein D, Nagy A, Schubert H, Weinberg G, Kitzelmann E, Schlögl R (1996) Z für Phys Ch 197:67–96
15. Czanderna AW (1966) J Phys Chem 70:2120
16. Bao X, Barth JV, Lehmpfuhl G, Schuster R, Uchida Y, Schlögl R (1993) Ertl G 284:14–22
17. Schubert H, Tegtmeyer U, Herein D, Bao X, Muhler M, Schlögl R (1995) Catal Lett 33:305–319
18. Rovida G, Pratesi F, Maglietta M, Ferroni E (1972) J Vacuum Sci Technol 9(2):769–799
19. Rovida G, Pratesi F, Maglietta M, Ferroni E (1974) Surf Sci 43:230–256
20. Bao X, Lehmpfuhl G, Weinberg G, Schlögl R, Ertl G (1992) J Chem Soc Faraday Trans 88(6):865–872
21. Schmidt WA, Frank O, Czanderna AW (1973) Phys Stat Sol A 16:127
22. Czanderna AW, Frank O, Schmidt WA (1973) Surf Sci 38:129–138
23. Janssen MMP, Moolhuysen J, Sachtler WMH (1972) Surf Sci 33:624–629
24. Barroo C, Austin JK, Bell DC (2019) Appl Surf Sci 487:1362–1365
25. Montemore MM, Montessori A, Succi S, Barroo C, Falcucci G, Bell DC, Kaxiras E (2017) J Chem Phys 146:214703
26. Barroo C, Montemore MM, Janvelyan N, Zugic B, Akey AJ, Magyar AP, Ye J, Kaxiras E, Biener J, Bell DC (2017) J Phys Chem C 121:5115–5122
27. Fowler RH, Nordheim DL (1928) Proc R Soc Lond Ser A 119:173–181
28. Forbes RG (1999) Ultramicroscopy 79:11–23
29. Bär T, Visart de Bocarmé T, Kruse N (2000) Surf Sci 454–456:240–245
30. Buatier de Mongeot F, Valbusa U, Rocca M (1995) Surf Sci 339:291–296
31. Campbell CT (1985) Surf Sci 157:43–60
32 Schmalzried H (1995) Chemical Kinetics of Solids. VCH Verlagsgesellschaft, Weinheim
33. Argyl MD, Bartholomew CH (2015) Catalysts 5:145–269
34 Lambeets SV, Visart de Bocarmé T, Perea DE, Kruse N (2020) J. Phys. Chem. Lett. 11(8):3144–3151
35. Montemore MM, Cubuk ED, Klobas JE, Schmid M, Madix RJ, Friend CM, Kaxiras E (2016) Phys Chem Chem Phys 18:26844–26853
36. Montemore MM, Madix RJ, Kaxiras E (2016) J Phys Chem C 120(30):16636–16640
37. Visart de Bocarmé T, Chau T-D, Tielens F, Andrés J, Gaspard P (2006) J. Chem. Phys. 125:054703
38. Tielens F, Andrés J, Chau T-D, Visart de Bocarmé T, Kruse N, Geerlings P (2006) Chem Phys Lett 421:433–438
39. Visart de Bocarmé T, Chau T-D, Kruse N (2007) Surf Interface Anal 39:166–171
40. Boronat M, Pulido A, Concepcion P, Corma A (2014) Phys Chem Chem Phys 16:26600
41. Montemore MM, Madix RJ, Kaxiras E (2016) J Phys Chem C 120:16636–16640
42. Deng X, Min BK, Guloy A, Friend CM (2005) J Am Chem Soc 127:9267–9270
43. Jacobs L, Barroo C, Gilis N, Lambeets SV, Genty E, Visart de Bocarmé T (2018) Appl Surf Sci 435:914–919
44. Gilis N, Jacobs L, Barroo C, Visart de Bocarmé T (2018) Top Catal 61:1437–1448